Turbulent Particle Dispersion in Electrostatic Precipitators

B.S. Choi, C.A.J. Fletcher

CANCES, University of New South Wales, Sydney 2052, Australia

ABSTRACT

The behaviour of charged particles in the turbulent gas flow in an electrostatic precipitator (ESP) is key information to optimise precipitator efficiency. This paper describes a strongly coupled calculation procedure for the rigorous computation of particle dynamics during electrostatic precipitation taking into account the statistical particle size distribution. The turbulent gas flow and the particle motion under electrostatic forces are calculated by using the commercial computational fluid dynamics (CFD) package FLUENT linked to a finite-volume solver for the electric field and ion charge. Particle charge is determined from local electrical conditions and cell residence time. Particle charge density and particle mobility are averaged in a control volume from the Lagrangian solution of the particle motion. The effects of particulate space charge on the electrical current flow and the particle transport are investigated. The calculated results for poly-dispersed particles are compared with those for mono-dispersed particles.

1. INTRODUCTION

An ESP is a device to separate fine particles from a flue gas by charging the particles and driving them toward the collecting plate by means of an electric field. The ESP has been used in the modern pulverised-coal fired power station and the cement industry since the beginning of the century.

Industrial electrostatic precipitation has very complex interaction mechanisms between the electric field, the fluid flow and the particulate flow. The numerical simulation of electrostatic precipitation is challenging especially when dust particles are heavily loaded in the gas stream. Electrostatic body force can produce a secondary gas flow well-known as electric wind in an ESP. Yamamoto and Velkoff (1981), Kallio and Stock (1992) solved governing equations for the fluid flow and the electric field to investigate the particulate-free secondary flow interaction between those fields. Charged dust particles migrate to the collecting plate due to Coulomb forces, but are also under the influence of momentum interaction with the gas flow in terms of aerodynamic drag. The motion of charged particles suspended in the gas stream was studied by Watanabe (1989) and Meroth et al. (1996). However, the effects of particulate space charge were neglected in their analysis. Heavily loaded particles generate high particle space charge and it can change the electric potential and the ion density distribution. Cristina and Feliziani (1991) included the particle space charge effect in the calculation of the electric field and current density distribution. They solved electrical equations only and perfect turbulent dispersion of particles was assumed to express particle concentration as a simple function of the distance from inlet of the ESP. They employed the saturation charge formula to determine the particle charge. Strong coupling of the governing equations describing the motion of ions, gas and particles including the effects of particle space charge and a novel description of particle charging are used in the present paper to predict an accurate particle motion in an industrial precipitator.

2. PHYSICAL MODELLING

2.1. Gas flow

Electrically induced turbulent flows have very wide spectrum of physically important length and time scales. These manifold scales limit the resolution of numerical analysis despite recent advances in computer technology. The most effective way for practical computations is to use averaged governing equations.

The gas flow is governed by the time-averaged conservation equations of mass and momentum. For steady, isothermal flow they have the following forms:

conservation of mass

$$\frac{\partial}{\partial x_k}(\rho u_k) = 0 \qquad (1)$$

conservation of momentum

$$\frac{\partial}{\partial x_k}\left(\rho u_i u_k - (\mu + \mu_t)\frac{\partial u_k}{\partial x_k}\right) = -\frac{\partial p}{\partial x_i} + f_{D_i} + \rho_{ion} E_i \qquad (2)$$

where ρ and ρ_{ion} are the mass density of the gas and the ion charge density, u is the gas velocity, f_D is the aerodynamic drag and E is the strength of the electric field. Turbulent viscosity μ_t is calculated from the solution of the conservation equations of turbulence kinetic energy and turbulence dissipation rate in the RNG $k-\varepsilon$ model (Yakhot and Orzag, 1986).

2.2. Particulate flow and particle charging

The particulate two-phase flow is described basically in two ways, namely the Lagrangian and the Eulerian methods. The Lagrangian approach treats the fluid phase as a continuum and calculates the trajectory of a discrete single particle from the balance of forces acting on the particle. The Eulerian approach treats the particulate phase as a continuum too. The conservation equations of mass and momentum are solved for both phases.

Both approaches have their advantages and disadvantages[Durst et el.,1984]. The Lagrangian approach provides a detailed information of the particulate flow, such as particle trajectories, individual particle velocities, and residence times. This method can calculate the particulate two-phase flow consisting of poly-dispersed particles. However, the Lagrangian approach, in general, has a limitation on the particle volume fraction so that the particulate phase is sufficiently dilute. The Eulerian approach has advantages in predicting highly concentrated two-phase flows. Turbulent mixing processes of the particles can be easily modelled in the Eulerian approach. Since the particulate two-phase flow in industrial electrostatic precipitators is sufficiently dilute and the particle size distribution is an important operating condition of an industrial ESP, the present study employs the Lagrangian approach.

Flyash particles are accelerated by the electrostatic force and the aerodynamic drag. When collision and coagulation between particles can be neglected, the equation of the particle motion is expressed as:

equation of particle motion

$$M_p \frac{dv_i}{dt} = q_p E_i + 3\pi\mu d_p (u_i - v_i) \times \left(1 + 0.15\mathrm{Re}_p^{0.687}\right) \qquad (3)$$

where M_p represents the particle mass, v_i the particle velocity, q_p the particle charge, $\mathrm{Re}_p = \rho|u - v|d_p/\mu$ particle Reynolds number and d_p the particle diameter.

Ions generated by the electric breakdown adhere to the particles suspended in the gas stream and charge them. The charging rate of the spherical particle by the field charging mechanism is given by (Cross, 1987):

particle charging

$$\frac{dq_p}{dt} = \frac{1}{\tau q_{\max}}(q_{\max} - q_p)^2. \qquad (4)$$

Here, τ is defined as the time taken for the particle to reach half the saturation charge, $\tau = 4\varepsilon_o/\rho_{ion} b_{ion}$, q_{max} is the maximum possible charge by the local electric field at the particle's location, $q_{\max} = \pi\varepsilon_o p_\varepsilon d_p^2 E$, and $p_\varepsilon = 3\varepsilon_r/(\varepsilon_r + 2)$. If the particle is unsaturated ($q_{p_o} < q_{max}$) at t=t_o, the equation (4) can be easily integrated for the time increment Δt by assuming that the values of ρ_{ion} and q_{max} are constant in the control volume. If the particle is sufficiently charged by the upstream electric field and has higher charge than the local saturation charge q_{max}, it will not acquire more charge in the current control volume.

2.3. Electric field and current flow

In spite of fundamental importance of the modelling of the corona discharge, the ionisation processes are very complex and difficult to predict. However, the corona region is limited to very small area in the vicinity of discharge electrode. For the economical computation of precipitation process the active corona zone is usually ignored.

The ion charge density and the strength of the electric field are determined by the current continuity equation and the Poisson equation for electric potential:

Poisson equation

$$\frac{\partial^2 \phi}{\partial x_k \partial x_k} = -\frac{\rho_{ion} + \rho_{pc}}{\varepsilon_o} \qquad (5)$$

current continuity equation

$$\frac{\partial}{\partial x_k}\Big(\rho_{ion}(b_{ion}E_k + u_k) - D_e\frac{\partial \rho_{ion}}{\partial x_k} + \rho_{pc}(b_p E_k + v_k)\Big) = 0 \qquad (6)$$

where ρ_{pc} is the particle charge density, b_{ion} and b_p are the mobilities of ions and charged particles, D_e is the effective diffusivity of ions.

The particle charge density and the particle mobility should be converted to Eulerian properties from the Lagrangian solution of particle motion to solve equations (5) and (6). The mass concentration of the particulate phase ρ_p and the particle charge density ρ_{pc} in a control volume are expressed in Eulerian form by the summation of the contribution of each particle:

$$\rho_p = \sum_{k=1}^{N_J} \dot{m}_p^k \Delta\tau_r^k / V_c \qquad (7)$$

$$\rho_{pc} = \sum_{k=1}^{N_J} q_p^k \frac{\dot{m}_p^k}{M_p^k} \Delta\tau_r^k / V_c \qquad (8)$$

where N_J represent the total number of particles visiting the control volume, $\dot{m}_p^k$ the mass flow rate from *k-th* particle injection point, $\Delta\tau_r$ the particle residence time in the cell and V_c the volume of the cell. The mass concentration and the particle charge density are calculated when the particle trajectories are computed. It is difficult to determine the cell-averaged particle mobility b_p for poly-dispersed particles. The averaged value of $b_p\rho_{pc}$ term is defined instead of the cell-averaged particle mobility b_p itself.

$$b_p\rho_{pc} = \sum_{k=1}^{N_J} b_p^k \rho_{pc}^k \qquad (9)$$

where

$$b_p^k = \frac{q_p^k}{3\pi\mu d_p^k\left(1 + 0.15\,\mathrm{Re}_p^{0.687}\right)} \qquad (10)$$

$$\rho_{pc}^k = q_p^k \frac{\dot{m}_p^k}{M_p^k} \Delta\tau_r^k / V_c. \qquad (11)$$

3. COMPUTATIONAL MODELLING

3.1 Method of solution

Turbulent fluid flow in an ESP is calculated by the commercial CFD package, FLUENT, using a finite volume method for the time-averaged Navier-Stokes equations closed by the k-ε turbulence model. The ion charge density and the electric field are obtained from the numerical solution of a Poisson equation for the electric potential and the current continuity equation by using a finite volume method. The user-defined subroutines are programmed and link the solution of the electric field with the FLUENT results. The Lagrangian equations of motion are integrated to compute the particle trajectories. Governing equations for the gas flow (u_i, p, k, ε), the particulate flow (v_i) and the electric field (ϕ, ρ_{ion}) are solved by iterative solver and they are cycled through the equation sequence at the global iteration for coupling between the equations.

3.2 Boundary conditions

Boundary conditions used in this calculation are summarised in Table 1.

Table 1 Applied boundary conditions

	gas velocity	particle motion	electric potential	ion charge density
Inlet	u_x=1.0m/s u_y=0.0m/s	v_x=1.0m/s v_y=0.0m/s	$\partial\phi/\partial n = 0$	$\partial\rho_{ion}/\partial n = 0$
Outlet	mass conservation	escape	$\partial\phi/\partial n = 0$	$\partial\rho_{ion}/\partial n = 0$
Collecting plate	no slip	trap	ϕ=0kV	$\partial\rho_{ion}/\partial n = 0$
wire electrode	no slip	reflect	ϕ=70kV	iterative adjusting

Concentrated particle space charge near the wire works to reduce the strength of the electric field and the corona current from the discharge electrode. Spatially different particle concentration results in different electric current at each wire. However, the strengths of the electric field at the surface of all wire electrodes have the same value satisfying Peek's formula (Cross, 1987). Ion charge density at the wire is adjusted by the iterative process until the calculated electric field agrees with that from Peek's formula.

$$\rho^{*}_{ion} = \rho^{n}_{ion}\left(\frac{E^n}{E_{Peek}}\right)^{\gamma} \qquad (12)$$

$$\rho^{n+1}_{ion} = (1-\omega)\rho^{n}_{ion} + \omega\rho^{*}_{ion}. \qquad (13)$$

where n indicates the iteration number, and ω the under relaxation factor. The exponent γ is determined by the ratio of electric current from the preceding two steps.

4. RESULTS

The model precipitator consists of three wires and two parallel plates. The wire-plate spacing is 0.1m and the wire-wire spacing is 0.15m. The total length of the precipitator is 0.45m. Three wire electrodes of 5mm diameter are 0.075m, 0.225m and 0.375m distant from inlet along the centre line. A finite volume grid of 122x34 cells is employed for the calculation. A densely packed grid is placed near the discharge electrode to represent accurately the strong gradients of the electric field as shown in Fig.1. Operating conditions of the precipitator are:

- Inlet velocities of gas and particles are 1.0m/s
- Density of solid particle is 1500kg/m^3
- Applied potential at wire is 70kV
- Particle diameter lies between 1 μm to 20 μm

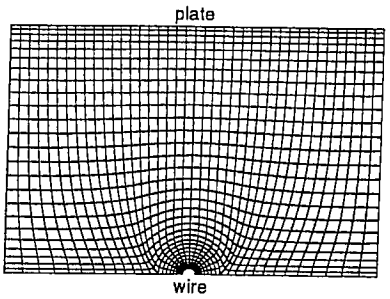

Fig.1. Part of computational mesh

Trajectories for the single-sized particles of $d_p = 2\mu m$ when the particulate concentration is negligible are shown in Fig.2. Particles passing the vicinity of the wire get highly charged by the highly stressed electric field and they move quickly toward the collecting plate. On the other hand, particles far from the wire drift to downstream because they have less charge. Due to the different development of charge, particle trajectories frequently cross in a banded area. High mass concentration is observed in the banded area in Fig.3 when the effects of particle space charge are included into the calculation of the electrical governing equations. The high concentration band could distort the electric field and feed-back to the particle transport.

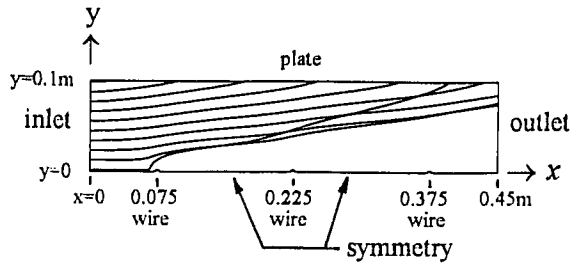

Fig.2. Particle trajectories for $d_p = 2\mu m$ & $(\rho_p)_{in} \approx 0g/m^3$

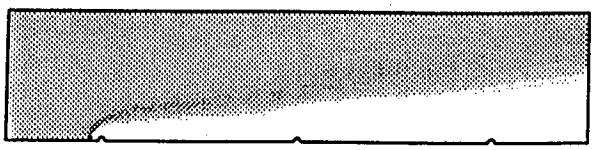

Fig.3. Particle mass concentration for $d_p = 2\mu m$ & $(\rho_p)_{in} = 1g/m^3$

Ion charge density distributions for the particle-free flow and the particle-loaded flow ($d_p = 2\mu m$ and $(\rho_p)_{in} = 1g/m^3$) are compared in Fig.4 and 5. The electric field without particle space charge produces a nearly symmetric pattern of ion charge density. Tiny deviation from symmetry is caused by the convection effect of the gas flow. On the other hand, suspended particles get charged as they move along the gas stream and high space charge density is generated near the wires due to the high particle concentration band shown in Fig.3. Even though the current flow by the charged particles is relatively small, space charge effects can be dominated by the particles because the particles stay in the interelectrode region for much longer period than ions (ion velocity is about 1000 times of particle migration velocity). Fig.5 indicates that highly charged particles distort the electric field and the current flow. Highly charged particles work to decrease the electric field near the wires, and then reduce the corona current from the discharge electrodes. Electric currents are 60.9%, 64.8% and 81.1% of the particle-free condition at the first, the second and the third wires, respectively.

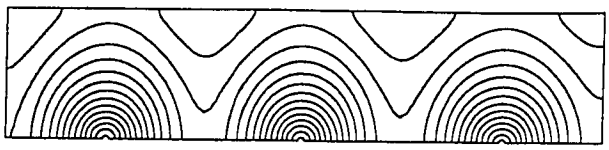

Fig.4. Ion charge density distribution for $(\rho_p)_{in} = 0g/m^3$ ($(\rho_{ion})_{max} = 45.7\mu C/m^3$, $(\rho_{ion})_{max} = 19.5\mu C/m^3$, contour interval=$1.87\mu C/m^3$)

Fig.5. Ion charge density distribution for $d_p = 2\mu m$ & $(\rho_p)_{in} = 1g/m^3$ ($(\rho_{ion})_{max} = 37.0\mu C/m^3$, $(\rho_{ion})_{max} = 11.7\mu C/m^3$, contour interval=$1.81\mu C/m^3$)

Particle mass concentration profiles at the exit of the precipitator are plotted in Fig.6 for $2\mu m$ particles with and without consideration of particle space charge in the calculation of electric potential and current. When the particle charge effects are included, the particle concentration profile is shifted to the centre line because of the reduction of corona current and the following decrease of Coulomb force. This implies that collection efficiency of an electrostatic precipitator can be over-predicted when particle space charge effects are neglected.

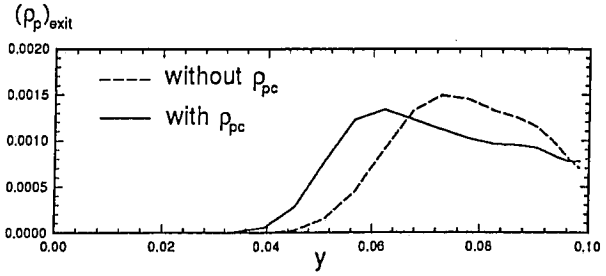

Fig.6. Particle mass concentration at exit for $d_p = 2\mu m$

Fig.7 shows the distribution of particle mass concentration for the particles of $d_p = 5\mu m$ and the mass concentration $(\rho_p)_{in} = 1g/m^3$. The larger particles are more highly charged and are

quickly removed at the collecting plate in the comparison with the smaller particles in Fig.3.

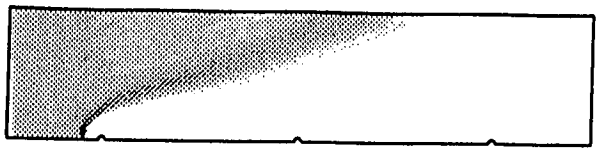

Fig.7. Particle mass concentration for $d_p = 5\mu m$ & $(\rho_p)_{in} = 1g/m^3$

Fig.8 shows the distribution of ion charge density for the particles of $d_p = 5\mu m$. The reduction of the corona current at each wire is less significant for the larger particle ($d_p = 5\mu m$) than the smaller particle ($d_p = 2\mu m$). The contribution by small particles to the particle space charge and the corresponding distortion of the electric field is more significant than large particles for two reasons. Particle charge density depends on the total surface area of particles. Smaller particles provide a large value of the total surface area for a given mass flow rate. The other contribution is caused by the fact that they can stay in the region closer to the discharge wires carrying a space charge for a longer time than larger particles.

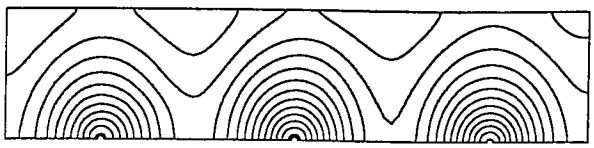

Fig.8. Ion charge density distribution for $d_p = 5\mu m$ & $(\rho_p)_{in} = 1g/m^3$ ($(\rho_{ion})_{max} = 45.3\mu C/m^3$, $(\rho_{ion})_{max} = 17.1\mu C/m^3$, contour interval=$2.01\mu C/m^3$)

Particle transport is calculated when two sizes of particles are mixed and released at the inlet of the ESP. Mass flow rate of each size particle is determined from the statistical particle size distribution for the pilot ESP (Lami et al., 1995). Particulate flows for three kinds of particle inflow, namely, premixed particles of $1\mu m$ and $5\mu m$ diameter (case A), single-sized particles of $d_p = 1\mu m$ (case B) and single-sized particles of $d_p = 5\mu m$ (case C) are compared. The contribution of small particles to distortion of the electric current flow is larger than that of large particles for the poly-dispersed particulate flow same as the mono-dispersed particulate flow described in Fig.4, Fig.5 and Fig.8. Lami et al. (1995) also pointed out that space charge by small particles may be significant although they have only small portion of particle mass. Particle mass concentration is compared for the mono-dispersed particulate flow ($d_p = 5\mu m$; case C) and the mixed particulate flow ($d_p = 1\mu m + d_p = 5\mu m$; case A) in Fig.9 and Fig.10. Almost $5\mu m$ particles of the case C are removed before the third wire. On the other hand, a considerable amount of $5\mu m$ particles of the case A is remained in the gas with $1\mu m$ particles at the third wire location. It is concluded the above result that the behaviour of large particle is altered by the presence of small particles. Small particles are mainly responsible for the distortion of the electric current flow in the poly-dispersed particulate flow. Distortion of the current flow can reduce the charge of large particles and corresponding Coulomb force acting on the particles. This is an indirect interaction between two sizes of particles although direct interaction between the particles is negligible.

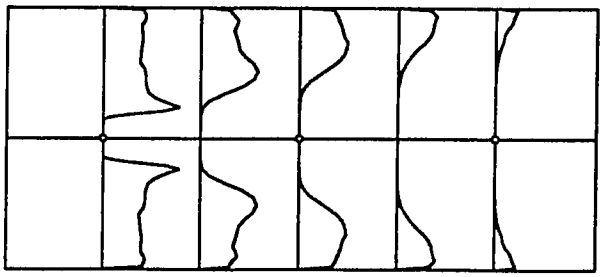

Fig.9. Particle mass concentration for mono-dispersed particles ($d_p = 5\mu m$, $(\rho_p)_{in} = 1.9g/m^3$)

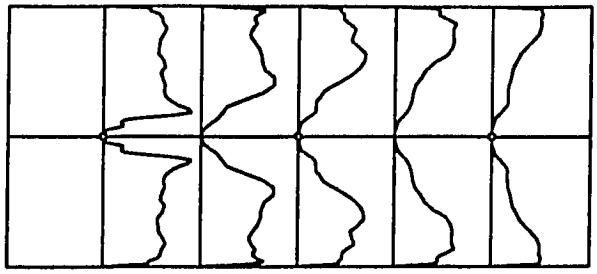

Fig.10. Particle mass concentration when two sizes of particles are mixed
($d_p = 1\mu m$, $(\rho_p)_{in} = 0.6g/m^3$ + $d_p = 5\mu m$, $(\rho_p)_{in} = 1.9g/m^3$)

5. CONCLUDING REMARKS

A strongly coupled calculation procedure is employed in the present study for complex interactions between the electric field, the gas flow and the particulate flow. A high particle concentration band is built up near the first wire due to the frequent particle trajectory crossing and long residence time in this region. Significant decrease of the corona current and the distorted distribution of ion charge due to the particle space charge are observed for small particles with relatively high dust loading. The effect of particle space charge on the particle transport is also considerable. For the poly-dispersed particulate flow, small particles can affect the behaviour of large particles through the distortion of the electric field.

REFERENCES

Yamamoto, T. and Velkoff, H.R., 1981, "Electrohydrodynamics in an electrostatic precipitator", J. Fluid Mechanics, 108, 1-18.

Kallio, G.A. and Stock, D.E., 1992, "Interaction of electrostatic and fluid dynamic fields in wire-plate precipitators", J. Fluid Mechanics, 240, 133-166.

Watanabe, T., 1989, "Calculation of flyash particle motion and its migration velocity in an electrostatic precipitator", IEEE Trans. Industry Applications, 2126-2136.

Meroth, A.M., Rastogi, A.K. and Schwab, A.J., 1996, "Numerical computation of the turbulent particulated flow in an electrostatic precipitator", Int. Symp. Filtration and Separation of Fine Dust, Vienna.

Cristina, S. and Feliziani, M., 1991, "Calculation of ionized fields in dc electrostatic precipitators in the presence of dust and electric wind", IEEE IAS Annual Meeting, 616-621.

Yakhot, V. and Orzag, S.A., 1986, "Renormalization group analysis of turbulence. I. Basic theory", J. Scientific Computing, 1, 3-51.

Durst, F., Milojevic, D. and Schonung, B., 1984, "Eulerian and Lagrangian predictions of particulate two-phase flows: a numerical study", Appl. Math. Modelling, 8, 101-115.

Cross, J., 1987, Electrostatics: Principles, Problems and Applications, Adam Hilger.

Lami, E., Mattachini, F., Gallimberti, I., Turri, R. and Tromboni, U., 1995, "A numerical procedure for computing the voltage-current characteristics in electrostatic precipitator configurations", J. Electrostatics, 34, pp.385-399.